Environmental Earth Sciences (2019) 78:524
https://doi.org/10.1007/s12665-019-8525-4

ORIGINAL ARTICLE

Dynamic response of land–atmosphere-coupling parameters to precipitation in the sparse-vegetated Asian summer monsoon transition zone

Qiang Zhang[1] · Zesu Yang[2] · Xiaocui Hao[1] · Hongyu Li[3]

Received: 14 August 2018 / Accepted: 2 August 2019 / Published online: 13 August 2019

Abstract

Land–atmosphere-coupling parameters usually relate to particular climatic conditions and seldom consider the influence of the inter-annual variability of precipitation. This results in large uncertainty in the estimation of land-surface physical variables. In the current study, observed data for five land–atmosphere-coupling parameters (surface albedo, soil thermal conductivity, aerodynamic roughness length, and the bulk transfer coefficients of momentum and sensible heat) were analysed and related to the inter-annual variability of precipitation on the Loess Plateau, China, from April 2006 to March 2013. This is an area with sparse vegetation. The results demonstrate that the land–atmosphere-coupling parameters are very sensitive to the inter-annual variability of precipitation. The surface albedo increased with increasing duration of snow cover. The other four parameters increased when annual effective precipitation (yearly sum of daily rainfall > 4 mm or daily snowfall > 0.1 mm) increased, and the sensitivity decreased when annual effective precipitation increased. Empirical relations between the five land–atmosphere-coupling parameters and the inter-annual variability of precipitation were derived via regression, with R^2 values of 0.67, 0.85, 0.93, 0.99, and 0.95, respectively. The land-surface physical variables calculated with dynamic land–atmosphere-coupling parameters (considering the inter-annual variability of precipitation) were much closer to the observed data than those calculated with static land–atmosphere-coupling parameters. The relative error was reduced by > 80% in years with low precipitation. This indicates that the inter-annual variability of precipitation has a significant impact on the land-surface physical variables. The results demonstrate that land–atmosphere-coupling parameters, which take into account inter-annual variability of precipitation, provide a more realistic representation of the land surface.

Keywords Land–atmosphere-coupling parameters · Inter-annual variability of precipitation · Land-surface physical variables · Sparse vegetation

Introduction

Land-surface processes are an important part of the interaction among the various components of the climate system, and they reflect exchanges of momentum, energy, and mass between the land surface and the atmosphere. They are also closely related to the weather and climate through feedback mechanisms (Zeng et al. 2003). Land-surface processes actively respond to adjustments in atmospheric circulation and changes in external forcing. Changes in weather and climate substantially influence land-surface processes (Huang 2006; Zhang et al. 2000). Inter-annual variability of precipitation has a large impact on land-surface properties and may cause inter-annual changes in land–atmosphere-coupling parameters. As land–atmosphere-coupling parameters are often used to calculate land-surface physical variables,

✉ Zesu Yang
zesuyang@outlook.com

[1] Key Laboratory of Arid Climatic Change and Reducing Disaster of Gansu Province, Key Open Laboratory of Arid Climatic Change and Disaster Reduction of CMA, Institute of Arid Meteorology, CMA, Lanzhou, Gansu, China

[2] Plateau Atmosphere and Environment Key Laboratory of Sichuan Province, College of Atmospheric Sciences, Chengdu University of Information Technology, Chengdu, Sichuan, China

[3] Hebei Climate Center, Hebei Provincial Meteorological Administration, CMA, Shijiazhuang, Hebei, China

inter-annual variability of precipitation, in turn, has a significant influence on land-surface physical variables. This leads to profound changes in land-surface energy and water processes (Zhao 2002; Li and Zhang 2003; Liu 2004). This influences terrestrial ecological processes and water cycles (Gao et al. 2004; Ma et al. 2008).

The northern boundary of the Asian summer monsoon is a region with a unique climate. Because of large spatial variation of precipitation, it is transition zone, from a southeast humid climate to northwest arid climate (Tang et al. 2007) and also from broadleaved deciduous forest in the southeast to typical desert steppe in the northwest (Ou and Qian 2006). The precipitation in this region has an average inter-annual variability > 30% (Hu and Qian 2007). These climatic characteristics affect land-surface features, such as the condition of vegetation and soil moisture content. Thus, land-surface processes are sensitive to change in precipitation.

The Loess Plateau is located in the Asian summer monsoon transition zone (Zhang and Wang 2008). The precipitation here is extremely variable and can be two to five times higher in wet years than in dry years (Lin and Wang 2007). The inter-annual variability of precipitation has a distinct influence on land-surface properties in this area. The land surface displays an aridification and desertification trend, as a result of decreasing precipitation over recent decades (Sun et al. 2005; Zhang et al. 2008; Huang et al. 2015). The changing land-surface properties are, in turn, altering the land–atmosphere-coupling parameters that describe land-surface energy and water transfer (Zhang et al. 2013a). The land-surface coupling parameters on the Loess Plateau are very sensitive to the inter-annual variability of precipitation, and land–atmosphere-coupling parameters show more inter-annual variability in this region (Zhang et al. 2013b).

Grasslands and deserts each comprise 25% of the Earth's surface. With the dominant surface type of sparse vegetation (Hu et al. 2004), the area of grassland and desert is about 41,600 km^2 and 28,080 km^2 in China, respectively. The properties of land surfaces with sparse vegetation are significantly influenced by the amount of precipitation. The response of land–atmosphere-coupling parameters to the inter-annual variability of precipitation is particularly strong over a land surface with sparse vegetation (Hu et al. 2004). It is essential to study the relationships between the land–atmosphere-coupling parameters and the inter-annual variability of precipitation, over a surface with sparse vegetation (Zhang et al. 2009b).

Land–atmosphere-coupling parameters reflect the degree of land–atmosphere interaction and are often used to calculate the land-surface physical variables. Inter-annual variability of precipitation affects land–atmosphere-coupling parameters and, as a consequence, results in changes in the land-surface physical variables. This influence is probably stronger on land surfaces with sparse vegetation. Consideration of the inter-annual variability of precipitation under sparse vegetation conditions has the potential to improve the estimation of land-surface physical variables.

Previous studies of land-surface-coupling parameters have been limited to certain climates (Dickinson 1995). Land–atmosphere-coupling parameters were initially regarded as static (Dai et al. 2003). As understanding gradually improved (Nicholson 2015), many studies focused on the seasonal variation of land–atmosphere-coupling parameters (Liu et al. 2008; Rechid et al. 2009; Zhang et al. 2012a; Liu et al. 2015), and these initial short-term (< 1 year) dynamic studies improved modelled fluxes (Zhou et al. 2006; Li et al. 2012a, b; Zheng et al. 2015). However, dynamic changes caused by inter-annual variability of precipitation were ignored (Ek et al. 2003; Wang et al. 2011). The land–atmosphere-coupling parameters were biased towards values reconstituted by observation (Chen and Zhang 2009) and did not reflect the actual state of the surface. As a result of this restriction, the response of land-surface physical variables to the inter-annual variability of precipitation received little attention.

The first objective of this study is to determine the relationships between the land–atmosphere-coupling parameters and the inter-annual variability of precipitation. Thus, new insight into land–atmosphere feedbacks and their sensitivity to variations in inter-annual rainfall will be gained. This is a development of earlier work on static and short-term land–atmosphere-coupling parameters. The second objective of this study is to analyse the influence of inter-annual variability of precipitation on the land-surface physical variables. The Semi-arid Climate Observatory and Laboratory (SACOL) (Huang et al. 2008; Wang et al. 2010; Guan et al. 2009) was selected as a sparsely vegetated representative site (Zhang et al. 2012b). Based on the land-surface data of SACOL and conventional climate data from the nearby Yuzhong meteorological station, an analysis was done to assess the response of land–atmosphere-coupling parameters to the inter-annual variability of precipitation and response equations were established. Next, the land-surface physical variables were calculated using these response equations, and the influence of the inter-annual variability of precipitation on these physical variables was determined. This work has the potential to be used as a quantitative basis for improved surface layer analysis.

Data and methods

Study site

The SACOL of Lanzhou University is located in an area with sparse vegetation (Huang et al. 2008). It is the main observatory used in the experimental study of land-surface

processes, on the Chinese Loess Plateau (Zhang et al. 2009a). The observatory is situated on the Loess Plateau in China, in the centre of the Asian summer monsoon transition zone (Zhang et al. 2012c; Li et al. 2013) (Fig. 1) and is approximately 7 km from the Yuzhong state meteorological station. The annual mean precipitation is 369 mm which is typical of a semi-arid climate. The variation in annual precipitation rate is approximately > 35%. In a comparatively wet year, the annual precipitation may exceed 400 mm, characteristic of a semi-humid climate. As a consequence of

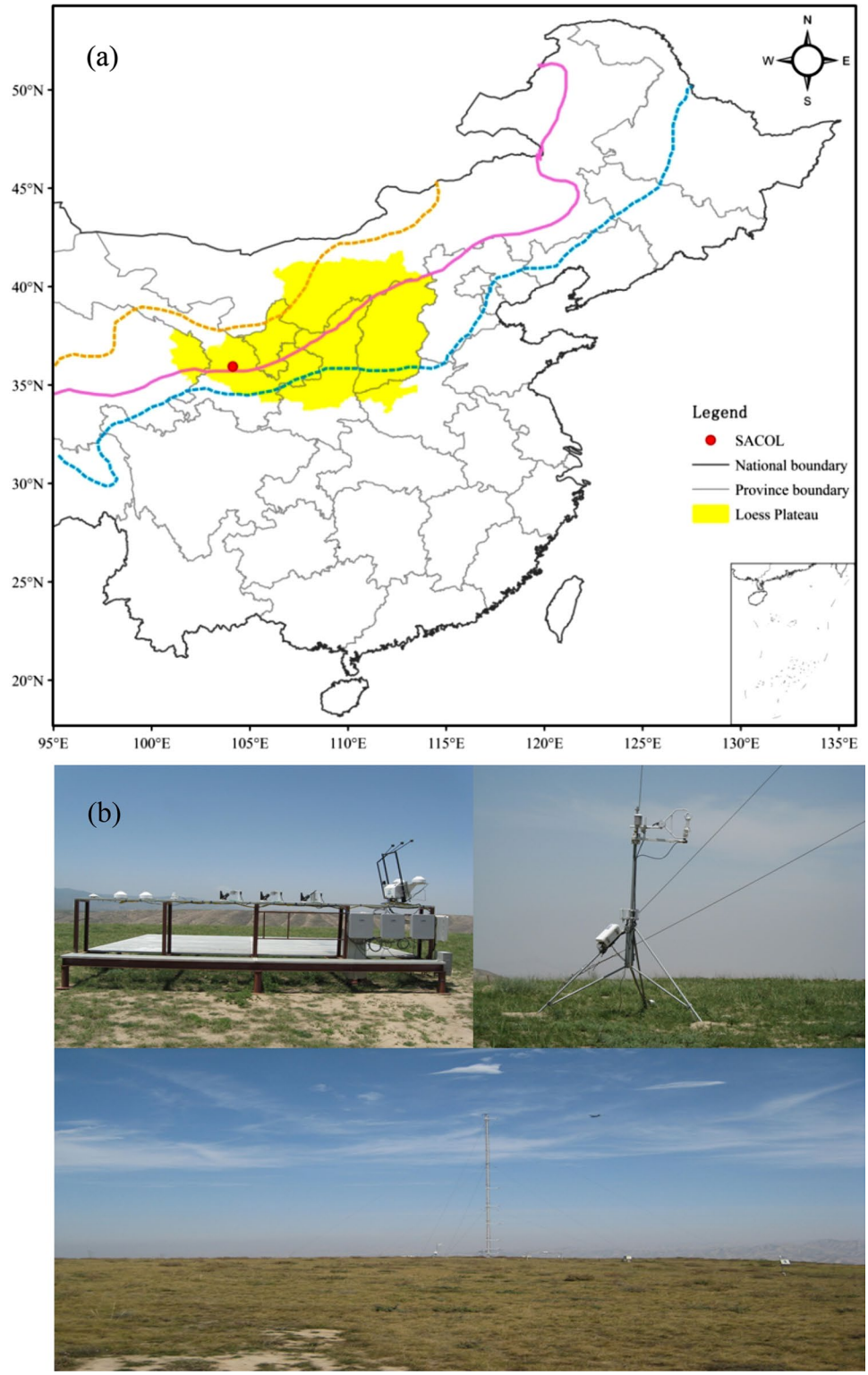

Fig. 1 **a** Location of the study site. The area between the yellow line and blue line is the Asian summer monsoon transition zone. **b** Views of the study site at the Semi-arid Climate Observatory and Laboratory of Lanzhou University

global climate change, the region is experiencing drying and warming (Huang et al. 2015), particularly during the cold season (Huang et al. 2012). The topography surrounding the observatory is characterized by undulating hills. The main soil type is loess: 36% sand, 43% silt, and 21% clay. The bulk density is 1.41 kg dm^{-3} and the pH of the soil water is 8 (Nachtergaele et al. 2008). The area of the observation field is approximately 0.08 km^2 and the terrain, where the measurements were taken is flat and covered with short grass (Fig. 1). The vegetation growth is entirely natural. This area is representative of how a sparsely vegetated land surface responds to inter-annual variability in precipitation (Li et al. 2012a, b).

The measuring instruments available at the SACOL are widely used and employ advanced techniques (Huang et al. 2008). Strict quality control of the data minimizes measurement errors. Recent studies have confirmed that the data from these instruments are very precise (e.g., Huang et al. 2008; Zhang et al. 2012a, 2013a). The SACOL has been in operation since 2006, and it is one of the few land-surface process observatories with relatively long-term, complete, and highly precise data. The SACOL has a large set of instruments for use in the observation of land-surface processes (Huang et al. 2008). The instruments used in this study included (1) an eddy covariance system set at a height of 3 m; (2) a surface radiation-monitoring system set at a height of 1.5 m; (3) seven layers of wind, air temperature, and air humidity measuring instruments set at heights of 1, 2, 4, 8, 12, 16, and 32 m; (4) six layers of soil temperature sensors buried at depths of 2, 5, 10, 20, 50, and 80 cm; (5) two layers of soil heat flux plates buried at depths of 5 and 10 cm; and (6) a barometric pressure sensor (see Table 1 for details of these instruments). The underlying surface is wide and flat with sparse vegetation, and thus, the surface area (1 m^2) observed by the radiation-monitoring system is typical of the land surface at this site.

Data

This study was conducted using the observed land-surface process data of the SACOL for the period from April 2006 to March 2013 and precipitation data from the Yuzhong national meteorological station for the period from April 1982 to March 2013. Figure 2 shows the inter-annual variability of precipitation over 30 years, including the study period. The average annual precipitation for the study years was 364 mm, which is close to the average annual precipitation over the 30-year period. The maximum and minimum annual precipitation during the study period was 548 and 280 mm, and the range of variation was 268 mm, which is about the same as that for the 30-year period. This indicates that the inter-annual variability of precipitation in the study period is a good representation of the inter-annual variability of precipitation over the 30-year period. Therefore, the land-surface process data at this site, for the period from 2006 to 2013, reflect the response of the land–atmosphere-coupling

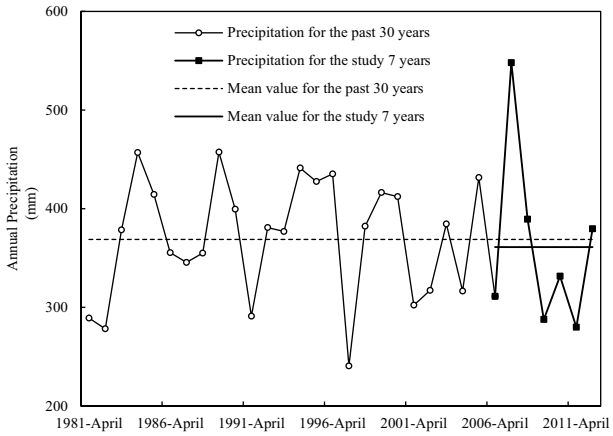

Fig. 2 Inter-annual variability of Yuzhong precipitation over a 30-year period

Table 1 Observations and instruments used at the SACOL site

Variables	Instrument	Model	Manufacturer
Wind speed	Anemometer	014A_L	Met One
Surface air temperature and humidity	Thermohygrometer	HMP45C-L	Met One
Pressure	Barometer	CS105	Vaisala
Upward and downward shortwave radiation	Pyranometer (shortwave flux)	CM21	Kipp & Zonen
Upward and downward longwave radiation	Pyrgeometer (longwave flux)	CG4	Kipp & Zonen
Soil heat flux	Soil heat flux plate	HFP01SC-L50	Hukseflux
Soil temperature	Soil temperature sensor	STP01-L50	Hukseflux
Latent heat flux, sensible heat flux, momentum flux, friction velocity	3D Sonic anemometer	CSAT3	Campbell
	Opened path infrared CO_2 and H_2O analyser	LI7500	Li-Cor

parameters to the inter-annual variability of precipitation, over the 30-year period.

To better characterize the annual precipitation, the beginning and end of a year were defined by the precipitation properties and characteristics of the water cycle, rather than the calendar year. One year was defined as the period from April 1 to March 31 of the following year. Although influenced by the Asian summer monsoon, the study region experiences snowfall in winter. The beginning of a year is characterized by the transition from snowfall to rainfall and from soil freezing to thawing. The period from April 1 to October 31 was defined as the rainfall period, or the warm season. The period from November 1 to March 31 was defined as the snowfall period, or the cold season. The effective precipitation was defined as rainfall > 4 mm day^{-1} or snowfall > 0.1 mm day^{-1} (Wang et al. 2013). The effective precipitation is that part of the precipitation that can be absorbed by the soil and can affect the properties of the land surface—for example, changing the soil moisture content.

Figure 3 illustrates the inter-annual variability of the annual precipitation, the annual effective precipitation, the annual rainfall, the annual snowfall, and the duration of snow cover, with maxima up to 236.9 mm, 227.1 m, 237.9 mm, 7.3 mm, and 137.5 h, respectively. The inter-annual variability of the annual precipitation, annual effective precipitation, and annual rainfall is fairly consistent. The small difference between the annual effective precipitation and the annual precipitation indicates that some of the precipitation events over the Loess Plateau have no effect on the soil moisture content. There is a large difference between the variation in annual snowfall and the duration of snow cover, because the duration of snow cover is also influenced by factors such as the duration of sunshine, wind speed, and intensity of the snowfall. After considering the mechanisms controlling the influence of precipitation on land–atmosphere-coupling parameters, the annual effective precipitation and duration of snow cover were chosen as the precipitation factors.

Figure 4 shows the relationship between annual effective precipitation and annual mean soil volumetric water content (VWC), during the study period. The variation in VWC of the 5, 10, 20, 40, and 80 cm layers is similar to that of annual effective precipitation (Fig. 4a). This indicates that they are highly correlated, with correlation coefficients of

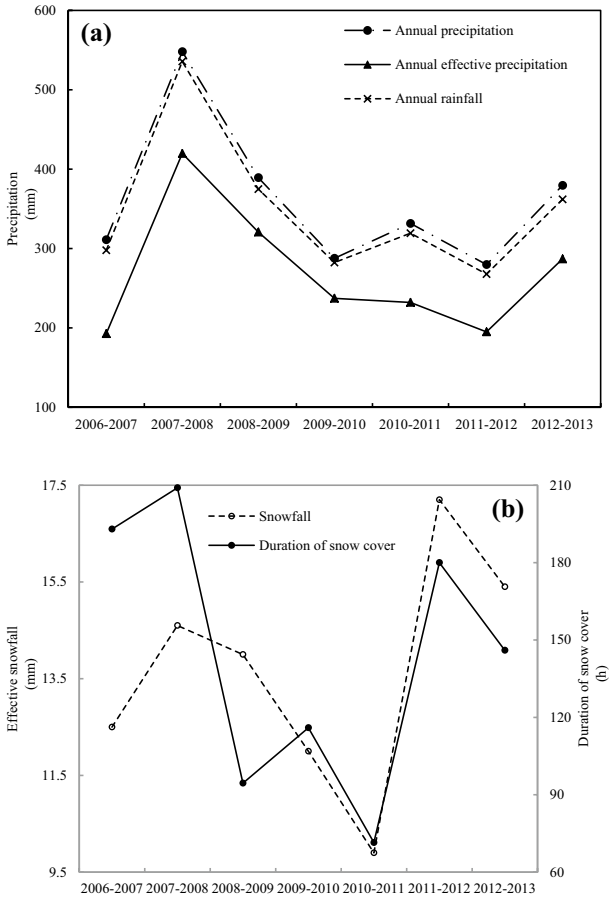

Fig. 3 **a** Inter-annual variability of annual precipitation, annual effective precipitation, and annual rainfall. **b** Inter-annual variability of annual snowfall and duration of snow cover

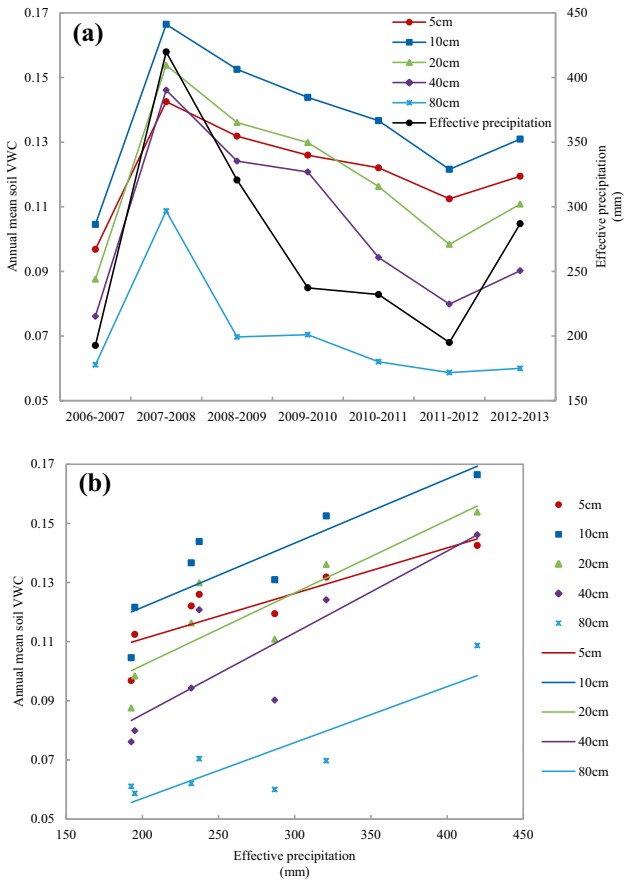

Fig. 4 Relationship between annual effective precipitation and annual mean soil VWC

0.859, 0.864, 0.873, 0.856, and 0.867 (Fig. 4b), respectively. Therefore, annual effective precipitation directly determined annual soil VWC. Soil VWC is an important influence on land–atmosphere-coupling parameters, and therefore, annual effective precipitation has a profound impact on land–atmosphere-coupling parameters.

To highlight the inter-annual variability of precipitation, the annual effective precipitation variability was defined as the ratio of the annual effective precipitation anomaly to the annual effective precipitation averaged over 30 years:

$$f_{\mathrm{pe}} = \frac{p_{\mathrm{te}} - \overline{p_{\mathrm{te}}}}{\overline{p_{\mathrm{te}}}}, \tag{1}$$

where f_{pe} is the dimensionless annual effective precipitation variability, p_{te} is the annual effective precipitation (mm), and $\overline{p_{\mathrm{te}}}$ is the annual effective precipitation (mm) averaged over 30 years. Similarly, the snow cover duration variability was defined as the ratio of the duration of snow cover anomaly to the duration of snow cover averaged over 30 years:

$$f_{\mathrm{s}} = \frac{p_{\mathrm{s}} - \overline{p_{\mathrm{s}}}}{\overline{p_{\mathrm{s}}}}, \tag{2}$$

where f_{s} is the dimensionless snow cover duration variability, p_s is the duration (h) of snow cover, and $\overline{p_{\mathrm{s}}}$ is the duration (h) of snow cover averaged over 30 years. Figure 5 compares the annual effective precipitation variability between Yuzhong station and the national mean, during the study period. National mean annual effective precipitation variability fluctuates within 0.15 and has a relatively small range, whereas annual effective precipitation variability at Yuzhong station is greater than 0.15 in almost all years and has a large range, with the largest value being 0.51 in 2007. Therefore, the study site has large annual effective precipitation variability, and this enhances the influence of annual effective precipitation variability on land–atmosphere-coupling parameters. In this study, a detailed analysis of the response of land–atmosphere-coupling parameters to annual effective precipitation variability is performed. Beijing time was used in this study.

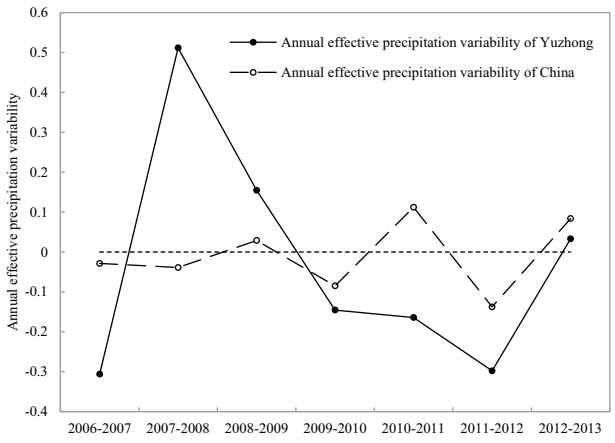

Fig. 5 Comparison of annual effective precipitation variability between the Yuzhong station and the national mean

Calculation of land–atmosphere-coupling parameters

The surface albedo, soil thermal conductivity, aerodynamic roughness length, and bulk transfer coefficient are the main land–atmosphere-coupling parameters in land-surface processes. The surface albedo is the ratio of the radiation reflected from the surface to the radiation incident on the surface and was defined by Zhang and Huang (2004) as

$$\alpha = R_{\mathrm{su}}/R_{\mathrm{sd}}, \tag{3}$$

where R_{su} (W m^{-2}) is the upward directed shortwave radiation at the surface (also known as reflected radiation) and R_{sd} (W m^{-2}) is the downward directed shortwave radiation.

The soil thermal conductivity represents the soil's ability to transfer heat and was defined by Zhang and Huang (2004) as

$$\lambda \mathrm{s} = -G/(\partial T_{\mathrm{g}}/\partial z), \tag{4}$$

where λs is the soil thermal conductivity (W m^{-1}°C^{-1}), z is the soil depth (m), G is the soil heat flux (W m^{-2}), and T_{g} is the soil temperature (°C). The values of G and T_{g} can be measured directly.

The aerodynamic roughness length is an important dynamic parameter, representing the height from the ground at which the wind speed theoretically becomes zero. It is determined by the following formula (Chen et al. 1993):

$$z_0 = (z-d)\mathrm{e}^{-\left(\kappa\frac{u}{u_*}+\psi_{\mathrm{m}}(\zeta)\right)}, \tag{5}$$

where z_0 is aerodynamic roughness length (m), z is the height of the eddy covariance system measurement, d is the zero plane displacement (m), u is the wind speed at height z, and u_* is the friction velocity (m s^{-1}). The values of u and u_* can be measured directly. Here, ψ_{m} is the stability correction function (Monin and Obukhov 1959) and can be expressed as

when $\zeta < 0$

$$\psi_{\mathrm{m}}(\zeta) = \ln\left[\frac{1+x^2}{2}\right] + 2\ln\left(\frac{1-x}{2}\right) - \tan^{-1}(x) + \frac{\pi}{2}, \tag{6}$$

$$x = (1-16\zeta)^{\frac{1}{4}}, \tag{7}$$

when $\zeta \geq 0$,

$$\psi_{\mathrm{m}}(\zeta) = -5\zeta, \tag{8}$$

where ζ is the Monin–Obukhov stability parameter. This is a dimensionless quantity and can be calculated by

$$\zeta = \frac{z-d}{L}, \tag{9}$$

where L is the Monin–Obukhov length, which can be calculated from observations (Oke 1978).

The bulk transfer coefficients of momentum and sensible heat are key parameters in the energy exchange between the land surface and atmosphere (Stull 2005) and can be calculated with

$$C_{\mathrm{d}} = (u_*/U)^2, \tag{10}$$

$$C_{\mathrm{h}} = \frac{H_{\mathrm{s}}}{\rho c_{\mathrm{p}} U(\theta_s - \theta_a)}, \tag{11}$$

where C_{d} and C_{h} are the dimensionless bulk transfer coefficients for momentum and sensible heat; ρ is the air density (kg m^{-3}), c_{p} is the specific heat capacity of dry air at a constant pressure (m^2 s^{-2} K^{-1}), H_{s} is the sensible heat flux in the surface layer (W m^{-2}), and θ_{s} and θ_{a} (K) are the potential temperature of the surface and atmosphere. The values of H_{s} and θ_{a} can be directly observed directly with the eddy covariance system. The value of θ_{s} can be calculated with the following equation:

$$\theta_{\mathrm{s}} = T_{\mathrm{s}}\left(\frac{P_0}{P}\right)^{0.288}, \tag{12}$$

where T_{s} is surface temperature (K), P_0 is standard atmospheric pressure, and P is the actual atmosphere pressure (hPa). Here, T_{s} is calculated with the Stefan–Boltzmann law as follows:

$$\sigma T^4 = \xi\sigma T_{\mathrm{s}}^4 + (1-\xi)R_{\mathrm{ld}}, \tag{13}$$

$$R_{\mathrm{lu}} = \sigma T^4, \tag{14}$$

$$T_{\mathrm{s}} = \left(\frac{R_{\mathrm{lu}} - (1-\xi)R_{\mathrm{ld}}}{\xi\sigma}\right)^{1/4}, \tag{15}$$

where ξ is the surface emissivity (0.96 in this study), σ is the Stefan–Boltzmann constant (5.67×10^{-8} W m^{-2} K^{-4}), T is the radiative surface temperature (K), R_{lu} is the upward directed longwave radiation, and R_{ld} is the downward directed longwave radiation (W m^{-2}).

Data processing

Processing original data

The data from the eddy covariance measurements were processed for quality control and gap-filling as follows: (1) half-hourly data from periods with sensor malfunctions were deleted; (2) half-hourly data 1 h before or 1 h after rainfall were deleted; and (3) half-hourly data (xi) were deleted when $xi \geq (+4\delta)$ or $xi \leq (-4\delta)$, where δ is the standard deviation. A look-up table was used to fill missing data. The half-hourly data were then averaged over 1 year.

For all other data, the few outliers from the general pattern of the time series were deleted and the gaps in the data were filled by linear interpolation. Different statistical methods were applied to the different variables. The half-hourly radiation data were averaged for the snowfall period, the rainfall period, and over a whole year. The half-hourly data for the soil temperature, wind speed, and soil heat flux were averaged over a whole year. The annual precipitation was taken as the sum of the daily rainfall and daily snowfall. The annual rainfall was taken as the sum of the daily rainfall. The annual effective precipitation was taken as the sum of the daily effective precipitation (daily rainfall > 4 mm or daily snowfall > 0.1 mm). The annual snowfall was taken as the sum of daily snowfall. The duration of snow cover was taken as the sum of hours of snow cover.

Calculation of land–atmosphere-coupling parameters and land-surface physical variables

The land–atmosphere-coupling parameters were calculated with Eqs. (3)–(15), and the data were processed (see above) as the input. The land-surface physical variables—including the reflected radiation, soil heat flux, friction velocity, momentum flux, and sensible heat flux—were calculated using Eqs. (3), (4), (5), (10), and (11). The land–atmosphere-coupling parameters were calculated using Eqs. (16)–(20).

Probability distribution of land–atmosphere-coupling parameters

Land-surface properties, such as soil moisture, soil colour, vegetation cover, and vegetation height, may change in response to the inter-annual variability of precipitation. This will affect the primary land–atmosphere-coupling parameters, such as the surface albedo, soil thermal conductivity, roughness length, and bulk transfer coefficients (for momentum and sensible heat). Before investigating the response of land–atmosphere-coupling parameters to precipitation variability, the probability distribution of land–atmosphere-coupling parameters during the study period was determined.

Figure 6 shows the probability distribution of the five land–atmosphere-coupling parameters. Surface albedo ranges from 0.009 to 1, and its probability distribution curve is unimodal, with a peak probability at 0.2. The value of surface albedo is concentrated in the range of 0.15–0.3, and the cumulative probability of this interval is up to 94.09% (Fig. 6a). Soil thermal conductivity ranges from 0.2 to 3.2,

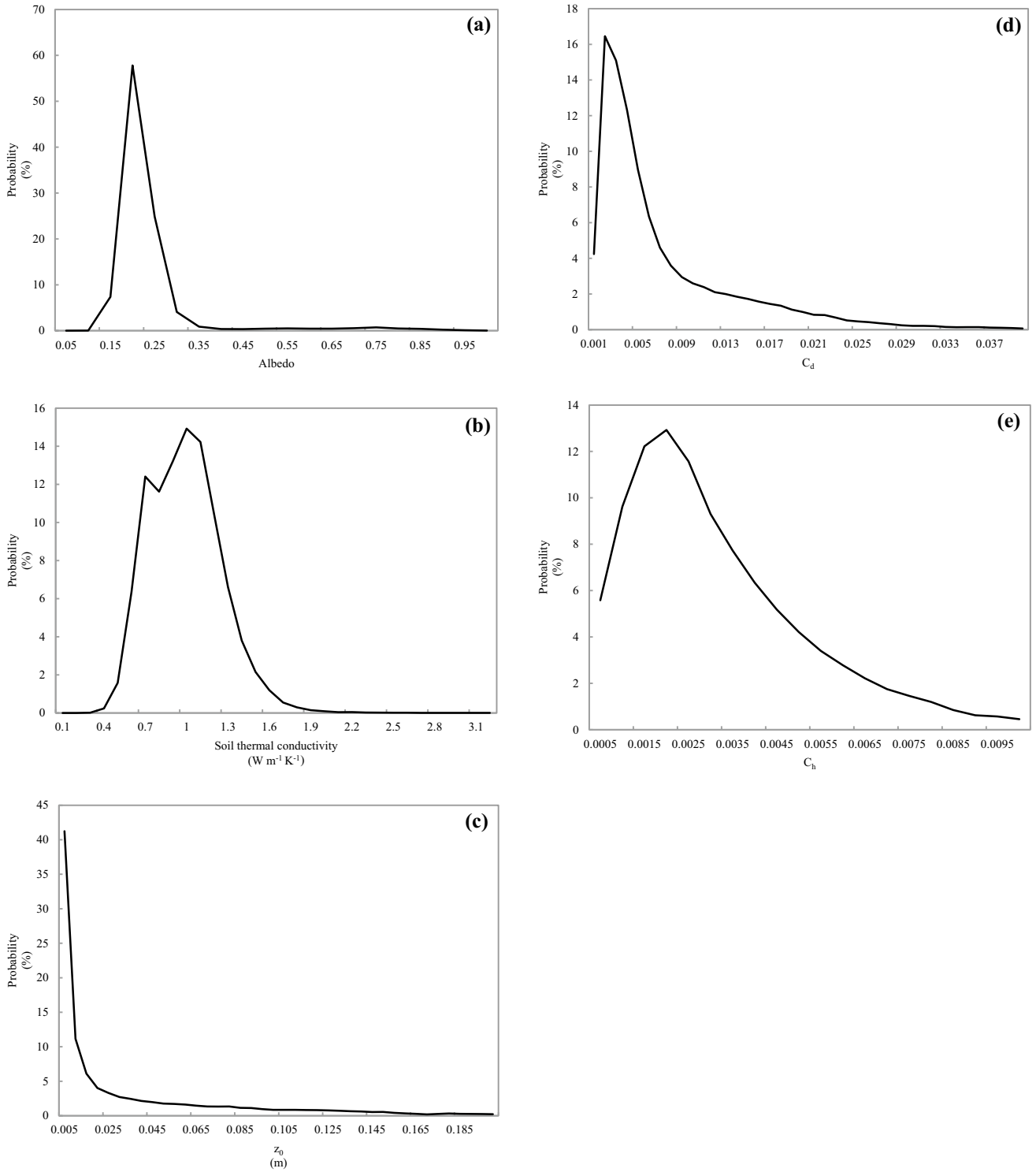

Fig. 6 Probability distribution of the five land–atmosphere-coupling parameters **a** surface albedo, **b** soil thermal conductivity, **c** roughness length, **d** bulk transfer coefficient of momentum, **e** bulk transfer coefficient of sensible heat

and its probability distribution curve is unimodal, with a peak value at about 1. The value of soil thermal conductivity is concentrated in the range of 0.6–1.3, and the cumulative probability of this interval is up to 89.76% (Fig. 6b). Roughness length ranges from 0 to 0.2, and the probability distribution curve is an inverse proportional function, with a peak probability at about 0.005. The value of roughness length is concentrated mainly between 0 and 0.045, and

the cumulative probability of this interval is up to 75.14% (Fig. 6c). The bulk transfer coefficient of momentum ranges from 0.0001 to 0.04, and the probability distribution curve is also unimodal, with a peak at 0.002. The value of the bulk transfer coefficient of momentum is concentrated mainly in the range from 0.001 to 0.01, and the cumulative probability of this interval reaches 77.18% (Fig. 6d). The bulk transfer coefficient of sensible heat ranges from 0.0001 to 0.01, and the probability distribution curve is unimodal, with a peak value at about 0.002. The value of the bulk transfer coefficient of sensible heat is concentrated mainly between 0.0005 and 0.0045, and the cumulative probability of this interval reaches 80.47% (Fig. 6e). This analysis demonstrates that although the five land–atmosphere-coupling parameters have a concentrated range with a cumulative probability of greater than 75%, the distribution range of each land–atmosphere-coupling parameter is still large. This indicates that the inter-annual variability of precipitation plays an important role in the dynamic change of land–atmosphere-coupling parameters.

Response of land–atmosphere-coupling parameters to the inter-annual variability of precipitation

Surface albedo

The surface albedo is sensitive to the inter-annual variability of precipitation (Zeng et al. 2011). As it is located in the centre of the summer monsoon transition zone, the Loess Plateau has two types of precipitation (rainfall and snowfall), which have different effects on the surface albedo.

Figure 7a shows the inter-annual variability of the average albedo during the rainfall period (April 1–October 31), the snowfall period (November 1–March 31), and the annual average albedo. The average albedo during the rainfall period was usually less than the mean albedo of croplands, whereas the average albedo in the snowfall period was sometimes larger than the mean albedo of deserts. The curve of the annual average albedo lies between the mean albedo of croplands and deserts (Zhang et al. 2002a, b; Stull 1988), in the range constrained by the climatic conditions. Figure 7a shows that the inter-annual variability of the average albedo in the rainfall period was very small. There does not appear to be a relation between the average albedo in the rainfall period and the annual effective precipitation. The inter-annual variability of the annual average albedo was consistent with the inter-annual variability of the average albedo in the snowfall period. The inter-annual variability of the average albedo in the snowfall period and the annual average albedo was not consistent with the annual effective precipitation, the annual

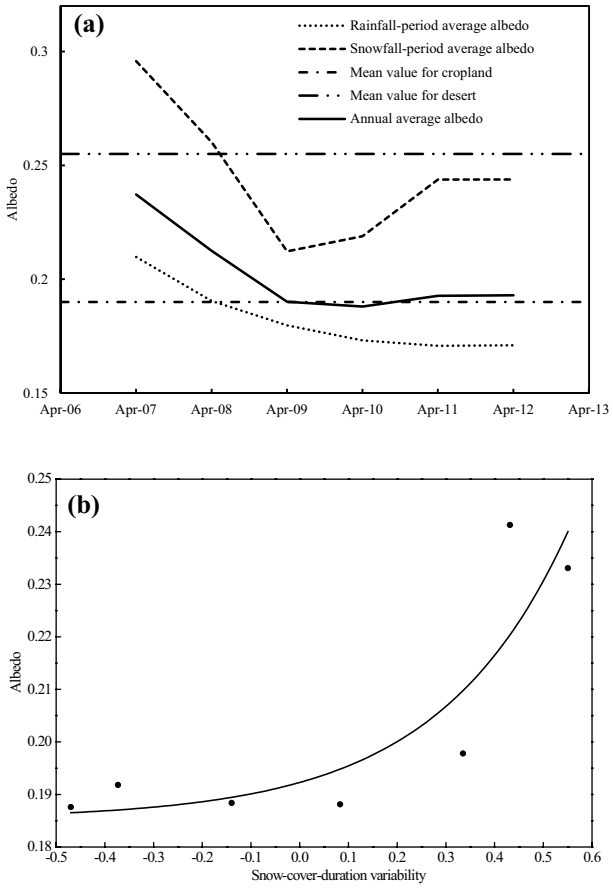

Fig. 7 **a** Inter-annual variability of average albedo during the rainfall period, the average albedo during the snowfall period, and the annual average albedo. **b** Regression of annual average albedo against snow cover duration variability

total precipitation, or the annual snowfall, but they were consistent with the inter-annual variability of the duration of snow cover. The albedo of snow is much larger than that of ground without snow, and snow melts very slowly on the Loess Plateau, as a result of low temperatures during the cold season. Therefore, the main factor affecting the inter-annual variability of the average albedo in the snowfall period is not the inter-annual variability of the annual snowfall, but the inter-annual variability of the duration of snow cover.

This situation is very different from that of warm and wet southeast China and cold and dry northwest China. In the arid areas of northwest China, although the temperature is very low during the cold season, the amount of snowfall is also low, because there is limited water. There is plenty of rainfall in southeast China, but weather conditions suitable for snow are rare, and even if there is snow, it melts quickly. Therefore, the annual snowfall in southeast and northwest China has a much smaller impact on the annual average albedo than it does in the Loess Plateau.

The inter-annual variability of the annual average albedo is dominated by the inter-annual variability of the duration of snow cover. This is because the inter-annual variability of the duration of snow cover dominates the inter-annual variability of the average albedo in the snowfall period. In addition, the inter-annual variability of annual average albedo is consistent with the inter-annual variability of the average albedo in the snowfall period. Figure 7b shows the regression of the annual average albedo against the snow cover duration variability, which is expressed as

$$\alpha_t = 0.00696e^{3.746f_s} + 0.185, \quad (16)$$

where α_t is the dimensionless annual mean albedo. The coefficient of determination (R^2) was 0.67 ($P < 0.01$), indicating that Eq. (16) fit the data well and could be used to characterize the response of the annual average albedo to the inter-annual variability of the duration of snow cover.

The annual snowfall is theoretically the primary factor influencing the duration of snow cover. Figure 8 shows the linear fit between the snow cover duration variability and the annual effective snowfall ($R^2 = 0.35$). The relatively poor regression is because the duration of snow cover is influenced not only by the annual snowfall, but also by other factors, such as the duration of sunshine, wind speed, and snowfall intensity.

Soil thermal conductivity

Precipitation affects the soil thermal conductivity by changing the soil moisture content. Snow does not affect the soil thermal conductivity directly, but it can affect it indirectly by changing the soil moisture content when it melts. The effective precipitation is that part of the precipitation which is converted to soil water in the root zone, and it is of great importance for the soil thermal conductivity. The annual effective precipitation (including the effective rainfall and effective snowfall) is, therefore, a critical factor in characterizing the influence of precipitation on the soil thermal conductivity.

Figure 9a shows the inter-annual variability of average soil thermal conductivity. The soil thermal conductivity was relatively high in the years with relatively large annual effective precipitation (see Fig. 3a). The mean soil thermal conductivity was about 0.92 W m^{-1} K^{-1}, with a maximum value close to 1 W m^{-1} K^{-1}, which is much higher than the mean value for deserts (0.177 W m^{-1} K^{-1}; Zhang et al. 2002a, b) and much lower than the mean value for croplands (1.58 W m^{-1} K^{-1}; Stull 1988). Figure 9b shows the regression of the annual average soil thermal conductivity plotted against the annual effective precipitation variability. The regression equation is

$$k_s = -0.00438e^{-13.179f_{pe}} + 1.002, \quad (17)$$

where k_s is the annual average soil thermal conductivity (W m^{-1} K^{-1}). The R^2 value of the regression was 0.85 ($P < 0.01$). Figure 9b shows that the annual average soil thermal conductivity was very sensitive to the annual effective

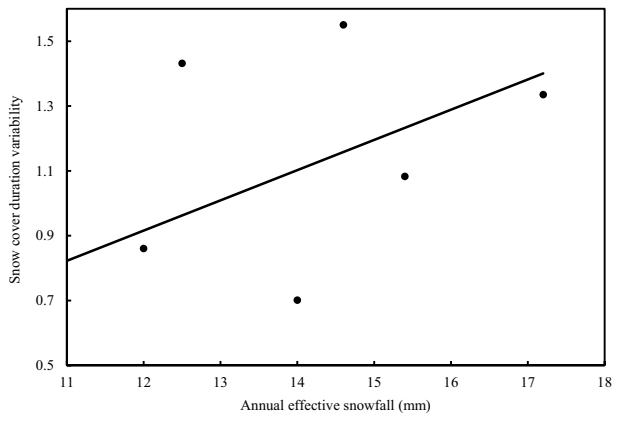

Fig. 8 Regression of snow cover duration variability against annual effective snowfall

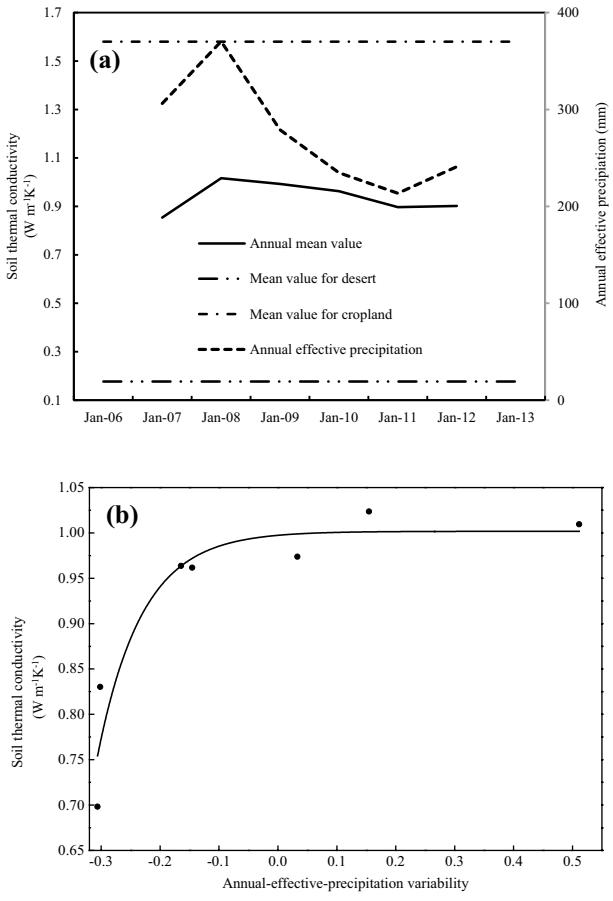

Fig. 9 **a** Inter-annual variability of soil thermal conductivity and **b** regression of soil thermal conductivity against annual effective precipitation variability

precipitation variability when this was relatively small. An increase of approximately 0.1 in the annual effective precipitation variability resulted in an increase in the soil thermal conductivity of > 0.2 W m^{-1} K^{-1}. However, the annual average soil thermal conductivity was not sensitive to the annual effective precipitation variability and remained essentially unchanged when this was > − 0.2. The relation between the effective precipitation and soil thermal conductivity was similar to that between the soil moisture content and soil thermal conductivity. The soil thermal conductivity increased with increasing soil moisture content when the soil moisture content was small, but did not change with increasing soil moisture content when it was relatively large.

Surface aerodynamic roughness length

The surface aerodynamic roughness length was significantly influenced by precipitation. The annual effective precipitation affects the surface aerodynamic roughness by changing plant growth. Precipitation changes the height and flexibility of the vegetation cover, leading to changes in the surface aerodynamic roughness. Figure 10a shows the distinct inter-annual variability in the annual average surface aerodynamic roughness. The maximum average surface aerodynamic roughness was 0.011 m in the year with the highest precipitation, and the minimum was 0.004 m in the year with the lowest precipitation. The maximum aerodynamic roughness length was more than twice the minimum value. This is because the Loess Plateau is situated at the Asian summer monsoon transition zone, and the annual effective precipitation just reaches the minimum water demand for vegetation growth. Vegetation is very sensitive to the annual effective precipitation, and even a small decrease in rainfall may have a substantial impact on vegetation status. The surface aerodynamic roughness length is, therefore, very sensitive to the annual effective precipitation. The aerodynamic roughness length is generally relatively large, as a result of tall, flourishing vegetation, in years with large amounts of precipitation. By contrast, the aerodynamic roughness length is smaller when vegetation is sparser and shorter, in years with lower precipitation. The annual average aerodynamic roughness length of these areas varies between that of deserts and farmland regions (Zhang et al. 2002a, b; Stull 2005), but is closer to that of desert regions. Figure 10b shows a plot of the regression of the annual average aerodynamic roughness length against the annual effective precipitation variability:

$$z_0 = -3.3797 \times 10^{-4} e^{-9.443 f_{pe}} + 0.0109, \quad (18)$$

where z_0 (m) is the aerodynamic roughness length. The R^2 value of the regression was up to 0.93 ($P < 0.01$). The aerodynamic roughness length was very sensitive to the annual effective precipitation variability when the effective precipitation was small. When the annual effective precipitation

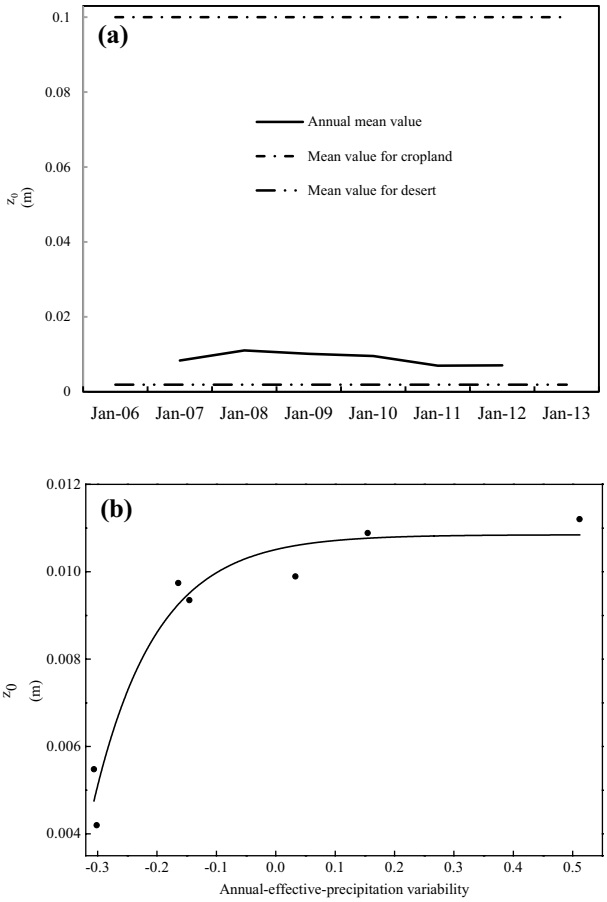

Fig. 10 **a** Inter-annual variability of aerodynamic roughness length and **b** regression of aerodynamic roughness length against annual effective precipitation variability

variability was > − 0.05, however, the roughness length was no longer sensitive to this variability and maintained a stable value of approximately 0.011.

The turning point of the sensitivity of the soil thermal conductivity to the annual effective precipitation variability was earlier than that of the sensitivity of the aerodynamic roughness length to this variability, and it occurred when the variability was very small. This is perhaps because the effective precipitation has a more direct effect on the soil thermal conductivity, by changing the soil moisture content, and has a more indirect effect on the aerodynamic roughness length. The effective precipitation first changes the soil moisture content, which, in turn, affects plant growth. The change in plant cover then affects the aerodynamic roughness length.

Bulk transfer coefficients

The effective precipitation affects the bulk transfer coefficient through its impact on the aerodynamic roughness length (Li et al. 2002). Figures 10b and 11a show the inter-annual variability of the bulk transfer coefficients of

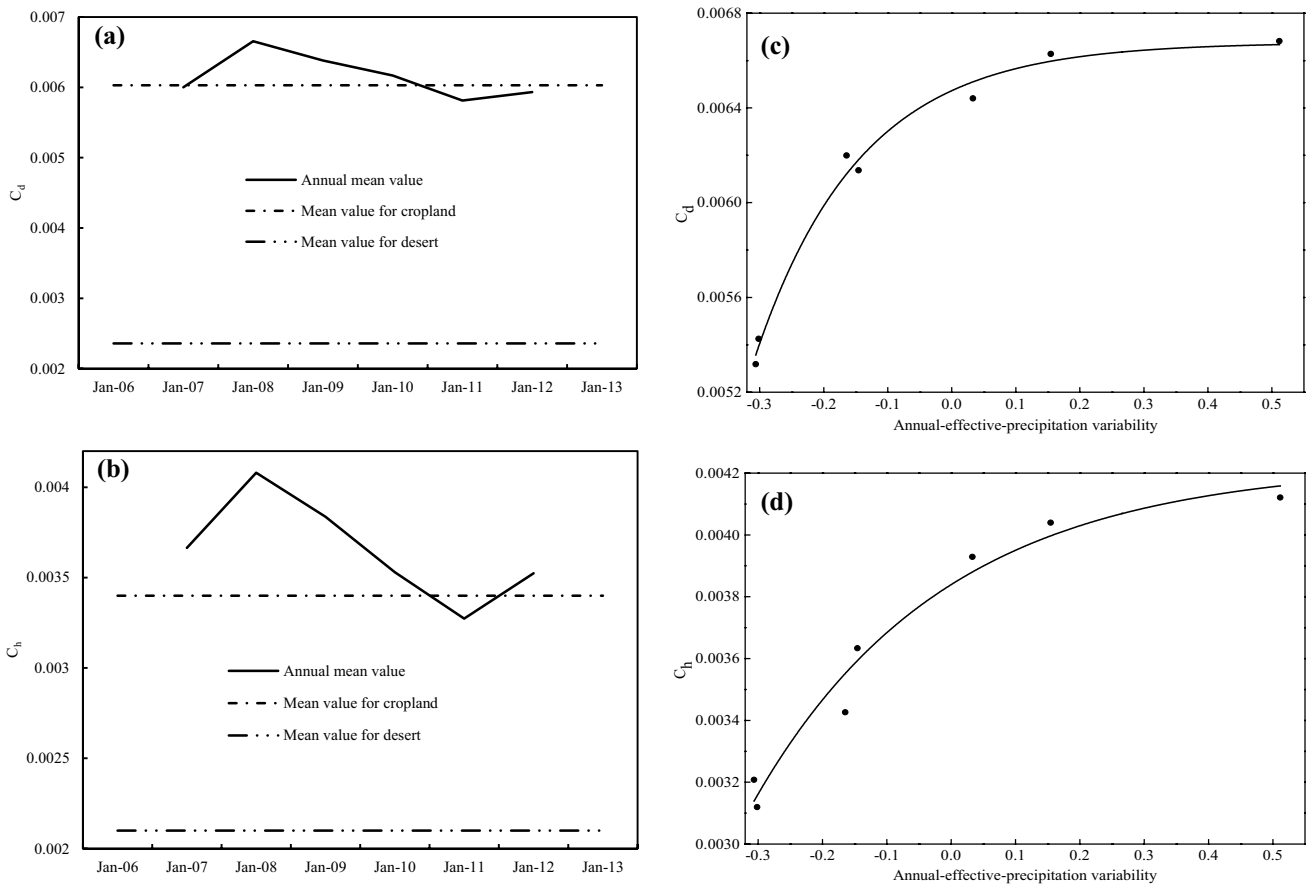

Fig. 11 Inter-annual variability of **a** bulk transfer coefficients of momentum and **b** sensible heat. Regression of bulk transfer coefficients of **c** momentum and **d** sensible heat against annual effective precipitation variability

momentum and sensible heat, respectively. The bulk transfer coefficient of momentum varied by about 0.0061. While the bulk transfer coefficient of sensible heat varied by about 0.0036, the bulk transfer coefficient of momentum was much larger than that of the sensible heat, which is similar to the results obtained in studies of arid deserts (Zhang et al. 2002a, b) and the Loess Plateau semi-arid areas (Wang et al. 2007). This shows that the bulk transfer coefficient of momentum predominates in arid and semi-arid regions. The majority of the bulk transfer coefficients of momentum and sensible heat were larger than the average values for cropland (Zhang et al. 2002a, b; Wang et al. 2007), and only the results for 2006 and 2011 were between the average values for croplands and deserts because of anomalously low precipitation. The Loess Plateau is surrounded by undulating hills, ridges, and mounds, and therefore, dynamic processes resulting from the topography intensify the momentum and sensible heat exchanges, between the land surface and atmosphere.

Figure 11c, d shows the regressions of the bulk transfer coefficients of momentum and sensible heat, against the annual effective precipitation variability. The bulk transfer coefficients of momentum and sensible heat were sensitive to the annual effective precipitation. They were relatively large in the years with large amounts of effective precipitation. This was mainly because the vegetation was lush in these years, which led to a relatively large roughness length and a relatively large bulk transfer coefficient. The regressions are

$$C_{\mathrm{d}} = -2.0342 \times 10^{-4} \mathrm{e}^{-6.106 f_{\mathrm{pe}}} + 0.00668, \quad (19)$$

$$C_{\mathrm{h}} = -3.8922 \times 10^{-4} \mathrm{e}^{-3.361 f_{\mathrm{pe}}} + 0.00423, \quad (20)$$

where C_{d} and C_{h} are the bulk transfer coefficients of momentum and sensible heat. The R^2 values of Eqs. (19) and (20) were 0.99 ($P < 0.01$) and 0.95 ($P < 0.01$), respectively. The bulk transfer coefficient was very sensitive to the annual effective precipitation variability and increased rapidly with an increase in this variability when the variability was < 0.1. The bulk transfer coefficient was not affected by the annual effective precipitation variability and maintained a stable value of 0.0066 for momentum and 0.0041 for sensible heat, when this was > 0.1.

The turning point of the bulk transfer coefficients (after which the bulk transfer coefficient is no longer sensitive to

the annual effective precipitation variability) (0.1) was larger than that of the roughness length (after which the roughness length is no longer sensitive to the annual effective precipitation variability) (− 0.05). This was presumably because the precipitation affects the bulk transfer coefficient indirectly, through its influence on the roughness length.

Impacts of inter-annual variability on the land-surface physical variables

Equations (16)–(20) give the response of the primary land–atmosphere-coupling parameters to the inter-annual variability of precipitation, and they describe the mechanisms of the inter-annual variability of the land–atmosphere-coupling parameters. This is an improvement upon static land atmosphere-coupling parameters, which did not consider the inter-annual variability of precipitation. Land–atmosphere-coupling parameters are used to estimate the land-surface physical variables. Therefore, in the future, these equations could be used to assess the impact of the inter-annual variability of precipitation on land-surface physical variables. This can be achieved by assessing the impact of the land–atmosphere-coupling parameters on the land-surface physical variables.

Five land-surface physical variables (reflected radiation, soil heat flux, friction velocity, momentum flux, and sensible heat flux) were calculated using Eqs. (3), (4), (5), (10), and (11). Two types of land-surface physical variables were calculated, with the two types of land–atmosphere-coupling parameters as inputs. The land–atmosphere-coupling parameters were calculated using Eqs. (16)–(20). Two types of land–atmosphere-coupling parameters were calculated using the different precipitation data as input. The first was calculated using the dynamic precipitation (considering the inter-annual variability of annual precipitation and using annual effective precipitation variability as the input). The second was calculated using the static precipitation (not considering the inter-annual variability of annual precipitation, but using the 7-year average of annual effective precipitation variability as the input). Next, the two types of calculated land-surface physical variables were compared with the observed data, to see which method was more consistent with the observations.

The surface albedo is mainly used to calculate the reflected radiation of the land surface. The reflected radiation was calculated using the albedo obtained from Eq. (16). Figure 12a compares the reflected radiation calculated using the dynamic precipitation (RD), reflected radiation calculated using the static precipitation (RS), and observed data. The RD results were closer to the actual observations than the RS results. The large snow cover duration variability reduced the deviation of RD from 19.54 and 15.7 W m^{-2}, to 8.64 and 2.8 W m^{-2}, for the years 2006 and

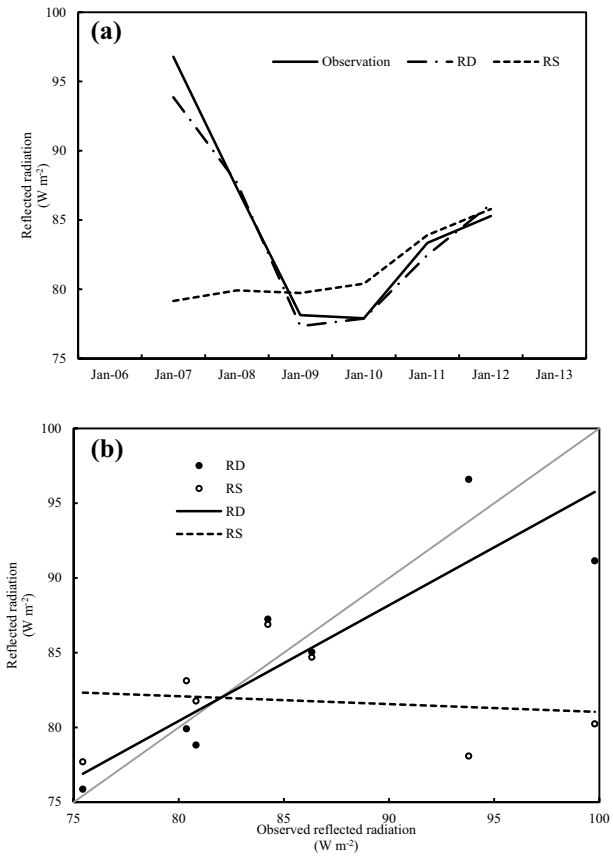

Fig. 12 **a** Comparison between reflected radiation calculated using the dynamic precipitation (RD), reflected radiation calculated using the static precipitation (RS), and the observed data. **b** RD and RS fitted to the observed data

Table 2 Correlation coefficient (r), root mean square error (RMSE), and residual error (RE) of reflected radiation, calculated using the dynamic precipitation (RD) vs. the observed data and static precipitation (RS) vs. the observed data

	r	RMSE (W m^{-2})	RE (W m^{-2})
RD vs. observed data	0.885	3.735	3.628
RS vs. observed data	0.131	9.650	7.712

The RE is the RMSE of the reflected radiation, calculated with the relationship of RD or RS fitted to the observed data. All the data were annual average values

2007, respectively. The relative error averaged for 2 years was reduced by approximately 80%. Figure 12b shows the relation between RD and RS linearly fitted to the observations. The results for RD were much closer to the 1:1 line than those of RS. Table 2 gives the correlation coefficient (r), the root mean square error (RMSE), and the residual error (RE, where RE is the RMSE of the reflected radiation calculated by the fit of RD or RS to the observed data). There was a significant improvement in the values of RD

vs. the observed data, compared with RS vs. the observed data: r increased by 0.754, RMSE decreased by 3.08, and RE decreased by 2.30 W m^{-2}. These results indicate that the calculated reflected radiation is closer to the observed value when the inter-annual variability of precipitation is considered.

Soil thermal conductivity is mainly used to calculate the soil heat flux. The soil heat flux was calculated using the soil thermal conductivity from Eq. (17). Figure 13a compares the soil heat flux calculated using the dynamic precipitation (GD), soil heat flux calculated using the static precipitation (GS), and observed data. The value of GD was closer to the observed values than GS. The improvement was relatively small, except for years 2006 and 2011, when the annual effective precipitation was small. This result is consistent with Fig. 9b, which shows that the soil thermal conductivity is very sensitive to the annual effective precipitation variability when the annual effective precipitation variability is small, and the soil thermal conductivity is not sensitive to the annual effective precipitation variability when this variability is relatively large. Figure 13b shows GD and GS linearly fitted to the observed data. Here, GD is closer to the 1:1 line than GS. Table 3 shows the correlation coefficient (r), RMSE, and RE. Here, RE is the RMSE of the soil heat flux, calculated with the relationship of GD or GS fitted to the observed data in Fig. 13b. Compared with the results for GS vs. the observed data, there was some improvement in the values of GD vs. the observed data: r increased by 0.04, the RMSE decreased by 0.061 W m^{-2}, and RE decreased by 0.022 W m^{-2}. Although the improvement was not significant, the calculated soil heat flux was closer to the observed value when the inter-annual variability of precipitation was considered.

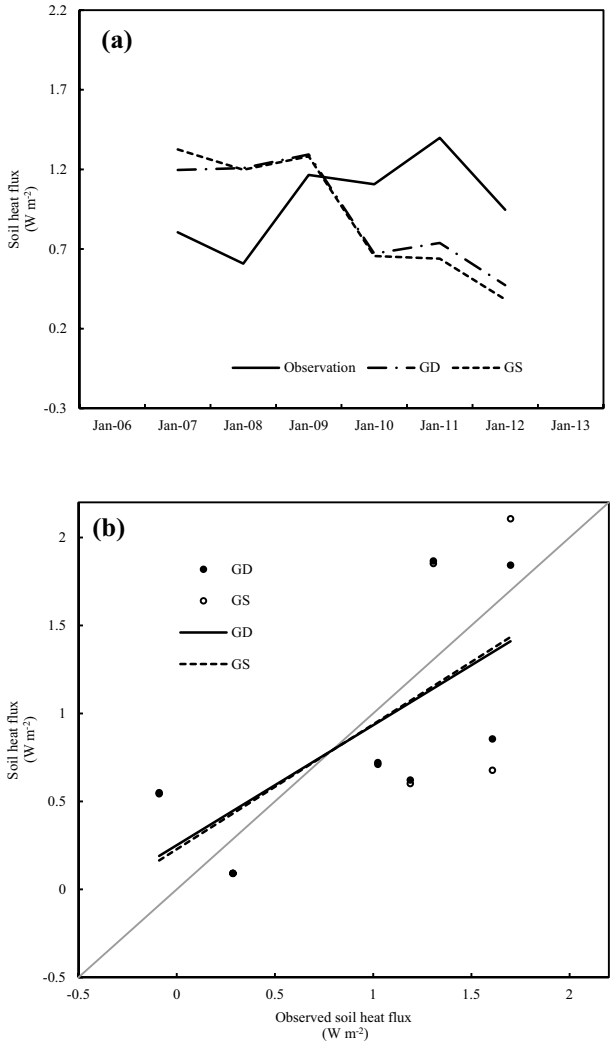

Fig. 13 **a** Comparison between soil heat flux calculated using the dynamic precipitation (GD), soil heat flux calculated using the static precipitation (GS) and the observed data. **b** GD and GS fitted to the observed data

The surface aerodynamic roughness length is usually used to calculate the friction velocity, which describes the friction between the land surface and the atmosphere. The friction velocity was calculated using the aerodynamic roughness length calculated with Eq. (18). Figure 14a compares the friction velocity calculated using the dynamic precipitation (UD), friction velocity calculated using the static precipitation (US), and observed data: UD was closer to the observed data than US. Compared with US, the deviation of UD decreased from 0.0173, 0.0144, and 0.142 m s^{-1} to 0.00416, 0.00264, and 0.00284 m s^{-1}, for years 2006, 2007, and 2008, respectively. The relative error averaged for 3 years was reduced by approximately 80%, showing a significant improvement. Figure 14b shows UD and US linearly fitted to the observations. Here, UD was closer to the 1:1 line than US. Table 4 gives the correlation coefficient (r), RMSE, and RE (RE is the RMSE of the soil heat flux calculated with the relationship of UD or US fitted to the observed data in Fig. 14b). Compared with US vs. the observed data, there was a significant improvement in UD vs. the observed dat: r increased by 0.584, RMSE decreased by 0.00826 m s^{-1}, and RE decreased by 0.00479 m s^{-1}. These results indicate that the calculated friction velocity was closer to the observed

Table 3 Correlation coefficient (r), root mean square error (RMSE), and residual error (RE) of soil heat flux calculated using the dynamic precipitation (GD) vs. the observed data and static precipitation (GS) vs. the observed data

	r	RMSE (W m^{-2})	RE (W m^{-2})
GD vs. observed data	0.679	0.501	0.454
GS vs. observed data	0.639	0.562	0.476

The RE is the RMSE of the reflected radiation calculated with the relationship of RD or RS fitted to the observed data

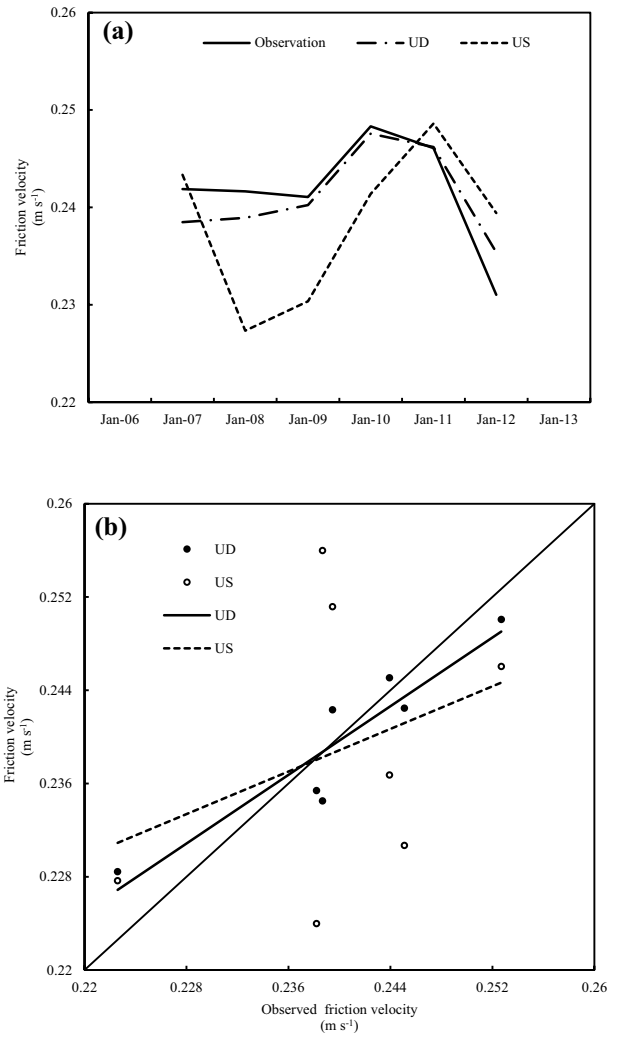

Fig. 14 **a** Comparison between friction velocity calculated using the dynamic precipitation (UD), friction velocity calculated using the static precipitation (US), and the observed data. **b** UD and US linearly fitted to the observed data

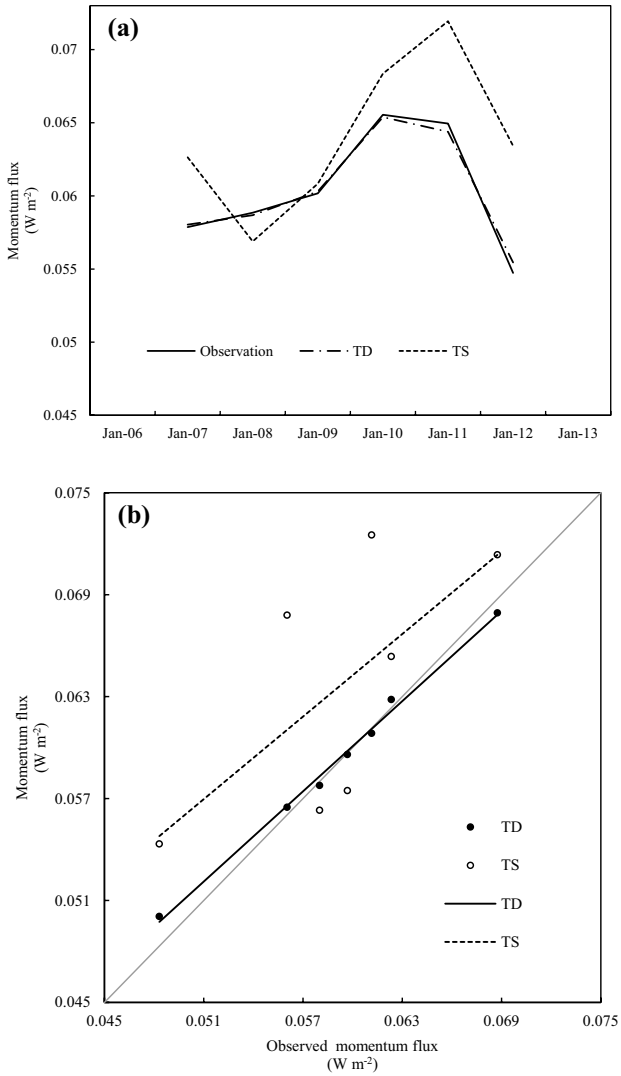

Fig. 15 **a** Comparison between momentum flux calculated using the dynamic precipitation (TD), momentum flux calculated using the static precipitation (TS) and the observed data. **b** TD and TS linearly fitted to the observed data

Table 4 Correlation coefficient (r), root mean square error (RMSE), and residual error (RE) of friction velocity calculated using the dynamic precipitation (UD) vs. the observed data and static precipitation (US) vs. the observed data

	r	RMSE (m s^{-1})	RE (m s^{-1})
UD vs. observed data	0.925	0.00344	0.00324
US vs. observed data	0.341	0.0117	0.00803

The RE is the RMSE of the reflected radiation calculated with the relationship of RD or RS fitted to the observed data

value when inter-annual variability of precipitation was considered.

The bulk transfer coefficient of momentum is usually used to calculate the momentum flux in the surface layer. The momentum flux was calculated using the bulk transfer coefficient of momentum calculated with Eq. (19). Figure 15a compares the momentum flux calculated using the dynamic precipitation (TD), momentum flux calculated using the static precipitation (TS), and observed data. Here, TD was closer to the observed data than TS. Compared with TS, the deviation of TD decreased from 0.0117 and 0.0114 N m^{-2} to 0.000445 and 0.000307 N m^{-2}, for years 2006 and 2011, respectively. The relative error averaged for 2 years was reduced by approximately 97%, a significant improvement. Figure 15b shows TD and TS linearly fitted to the observations: TD was closer to the 1:1 line than TS. Table 5 lists the correlation coefficient (r), RMSE, and RE (RE is RMSE of the soil heat flux calculated with the relationship of TD or TS fitted to the observed data in Fig. 15b). Compared with TS vs. the observed data, there

Table 5 Correlation coefficient (r), root mean square error (RMSE), and residual error (RE) of momentum flux calculated using the dynamic precipitation (TD) vs. observed data and static precipitation (TS) vs. observed data

	r	RMSE (N m^{-2})	RE (N m^{-2})
TD vs. observed data	0.997	0.000786	0.000427
TS vs. observed data	0.676	0.00683	0.00426

The RE is the RMSE of the reflected radiation calculated with the relationship of RD or RS fitted to the observed data

was a significant improvement in TD vs. the observed data: r increased by 0.321, RMSE decreased by 0.00604 N m^{-2}, and RE decreased by 0.00383 N m^{-2}. These results indicate that the calculated momentum flux was much closer to the observed value when the inter-annual variability of precipitation was considered.

The bulk transfer coefficient of sensible heat is usually used to calculate the sensible heat flux in the surface layer. The sensible heat flux was calculated using the bulk transfer coefficient of sensible heat calculated with Eq. (20). Figure 16a compares the sensible heat flux calculated using the dynamic precipitation (HD), sensible heat flux calculated using the static precipitation (HS), and observed data. Here, HD was closer the observed data than HS. Compared with HS, the deviation of HD decreased from 6.586 and 11.061 W m^{-2} to 0.753 and 0.622 W m^{-2}, for the years 2006 and 2011, respectively. The relative error averaged for 2 years was reduced by approximately 94%, showing significant improvement. Figure 16b shows HD and HS linearly fitted to the observed data: HD was closer to the 1:1 line than HS. Table 6 presents the correlation coefficient (r), RMSE, and RE (RE is the RMSE of the soil heat flux calculated with the relationship of HD or HS fitted to observed data in Fig. 16b). Compared with HS vs. the observed data, there was a significant improvement in HD vs. the observed data: r increased by 0.069, RMSE decreased by 4.531 W m^{-2}, and RE decreased by 1.258 W m^{-2}. These results indicate that the calculated sensible heat flux was closer to the observed value when the inter annual variability of precipitation was considered. The improvement was as significant as that of the momentum flux.

The comparison of the statically to dynamically derived land-surface physical variables used the same 7 years of data that were used to determine the relationships between the more fundamental land–atmosphere-coupling parameters and inter-annual variability of precipitation. This was necessary because of limited data. Therefore, the results cannot validate the relationships between the land–atmosphere-coupling parameters and the inter-annual variability of precipitation. Nevertheless, because the land-surface physical variables derived by static precipitation and those derived by dynamic precipitation used the same relationships, and

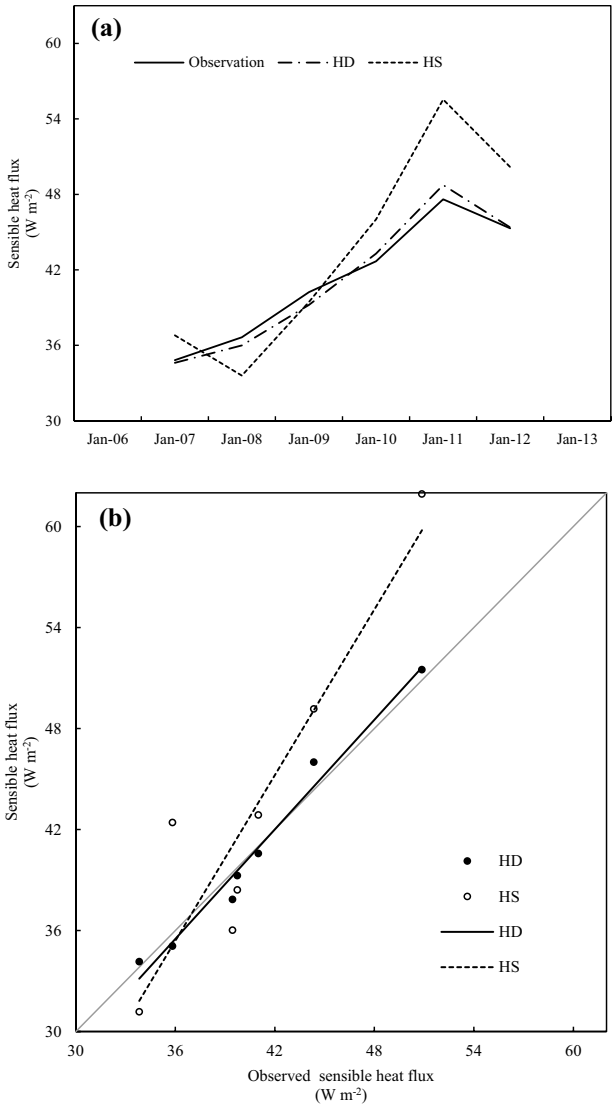

Fig. 16 **a** Comparison between sensible heat flux calculated using the dynamic precipitation (HD), sensible heat flux calculated using the static precipitation (HS), and the observed data. **b** HD and HS linearly fitted to the observed data

the input precipitation data (static and dynamic precipitation) were the only difference, the results effectively reflect the impact of the inter-annual variability of precipitation

Table 6 Correlation coefficient (r), root mean square error (RMSE), and residual error (RE) of sensible heat flux calculated using the dynamic precipitation (HD) vs. the observed data and static precipitation (HS) vs. the observed data

	r	RMSE (W m^{-2})	RE (W m^{-2})
HD vs. observed data	0.988	0.983	0.795
HS vs. observed data	0.919	5.514	2.053

The RE is the RMSE of the reflected radiation calculated with the relationship of RD or RS fitted to the observed data

on the land-surface physical variables. This is attributed to the impact of the land–atmosphere-coupling parameters on the land-surface physical variables when the inter-annual variability of precipitation is considered. Over semi-arid, sparsely vegetated areas, when compared with static precipitation, the calculation of the land-surface physical variables using dynamic precipitation yielded RMSE values of the estimated reflected radiation, soil heat flux, friction velocity, momentum flux, and sensible heat flux that were reduced by 61.3, 10.6, 70.6, 88.5, and 82.2%, respectively. These precipitation-based relationships have the potential to be used to validate the output of land-surface models, leading to a more accurate estimation of land-surface physical variables. The comparative analysis also indicates that dynamic land–atmosphere-coupling parameters that take the inter-annual variability of precipitation into consideration are better representation of the land surface.

Conclusions and discussion

Under sparse vegetation conditions, land–atmosphere-coupling parameters are strongly influenced by the inter-annual variability of precipitation. The Loess Plateau, located at the boundary zone influenced by the summer monsoon, has significant inter-annual variability in precipitation. This has a large impact on land-surface properties such as snow cover, vegetation conditions, and soil moisture. Land–atmosphere-coupling parameters are modulated by monsoon precipitation and show significant dynamic variability. Therefore, it is essential to consider the inter-annual variability of precipitation when using land–atmosphere-coupling parameters to calculate land-surface physical variables.

The land–atmosphere-coupling parameters of land-surface albedo, aerodynamic roughness length, soil thermal conductivity, and bulk transfer coefficient are responsive to inter-annual variability in precipitation. The aerodynamic roughness length, soil thermal conductivity, and bulk transfer coefficient increased with increasing annual effective precipitation. The surface albedo was relatively consistent with the albedo during the snowfall period and increased with increasing duration of snow cover, which was primarily modulated by the annual snowfall. The snow cover duration variability was defined as a precipitation factor, used to measure the impact of the inter-annual variability of snowfall on the surface albedo. The annual effective precipitation variability was defined as a precipitation factor, used to measure the impact of the inter-annual variability of effective precipitation on the other land–atmosphere-coupling parameters. The soil thermal conductivity, roughness length, and bulk transfer coefficients of momentum and sensible heat were regressed against the annual effective precipitation variability, and the surface albedo was regressed against the snow cover duration variability. The R^2 values for the regressions were 0.85, 0.93, 0.99, 0.95 and 0.67, respectively. The soil thermal conductivity, roughness length, and bulk transfer coefficients of momentum and sensible heat were sensitive to the annual effective precipitation variability, when this was relatively small. They were no longer sensitive to this variability and tended towards stable values when the variability was relatively large. This is because the mechanisms of their response to the soil moisture content were different. The turning points of the sensitivity of the land–atmosphere-coupling parameters, in response to the annual effective precipitation variability, were different. For the soil thermal conductivity, the turning point occurred at an annual effective precipitation variability of − 0.2, whereas the turning points for the roughness length and bulk transfer coefficients occurred at annual effective precipitation variabilities of − 0.05 and 0.1, respectively.

The land-surface physical variables calculated using dynamic precipitation were much closer to the observed data, than those calculated using static precipitation. The improvement was quite large in years with relatively small precipitation, and the relative error averaged for these years was reduced by up to 80%. The momentum flux and sensible heat flux were closer to the observed data and had almost no deviation when the inter-annual variability in precipitation was considered. This indicates that the error in the calculated land-surface variables was significantly reduced when the inter-annual variability in precipitation was considered, highlighting the fact that the influence of the inter-annual variability in precipitation on land–atmosphere-coupling parameters should not be ignored.

In conclusion, improved parameterizations for the primary land–atmosphere-coupling parameters, incorporating inter-annual variability in precipitation and with sparse vegetation, have been presented. However, because the data were only available for a certain time period and observations were from only one station, the results are limited. A systematic study, using a larger set of land-surface process data, would be valuable.

Acknowledgements We thank SACOL for providing the study data. This work was jointly supported by the Major Program of National Nature Science Foundation of China (41630426), Arid Found (IAM201701) and the Scientific Research Foundation of Chengdu University of Information Technology (KYTZ201734).

References

Chen F, Zhang Y (2009) On the coupling strength between the land surface and the atmosphere: from viewpoint of surface exchange coefficients. Geophys Res Lett 36(10):L10404

Chen JY, Wang JM, Guang TN (1993) An independent method to determine the surface roughness length. Chin J Atmos Sci 17(1):21–26

Dai YJ, Zhang XB, Dickinson RE, Baker I, Bonan GB, Bosilovich MG, Denning AS, Dirmeyer PA, Houser PR, Niu GY, Oleson KW, Schlosser CA, Yang ZL (2003) The common land model. Bull Am Meteorol Soc 84:1013–1023. https://doi.org/10.1175/BAMS-84-8-1013

Dickinson RE (1995) Land–atmosphere interaction. US Natl Rep Int Union Geod Geophys 1991–1994:917–922

Ek MB, Mitchell KE, Lin Y, Rogers E, Grunmann P, Koren V, Gayno G, Tarpley JD (2003) Implementation of Noah land surface model advances in the National Centers for Environmental Prediction operational mesoscale Eta model. J Geophys Res 108(22):8851. https://doi.org/10.1029/2002JD003296

Gao ZQ, Chae N, Kim J, Hong J, Choi T, Lee H (2004) Modeling of surface energy partitioning, surface temperature and soil wetness in the Tibetan prairie using the Simple Biosphere Model 2 (SiB2). J Geophys Res 109:D06102. https://doi.org/10.1029/2003JD004089

Guan X, Huang J, Guo N, Bi J, Wang G (2009) Variability of soil moisture and its relationship with surface albedo and soil thermal parameters over the Loess Plateau. Adv Atmos Sci 26(9):692–700

Hu HR, Qian WH (2007) Confirm of north edge of the East Asian summer monsoon. Prog Nat Sci 17:57–65

Hu YQ, Sun SF, Zheng YR, Zhang Q, Fu PJ, Zuo HC (2004) Review of study on interaction between underlying surface with sparse vegetation and atmosphere. Plateau Meteorol 23(3):281–296

Huang RH (2006) Progresses in research on the formation mechanism and prediction theory of severe climatic disasters in China. Adv Earth Sci 21:564–575

Huang JP, Zhang W, Zuo JQ, Bi JR, Shi JS, Wang X, Chang ZL, Huang ZW, Yang S, Zhang BD, Wang GY, Feng GH, Yuan JY, Zhang L, Zuo HC, Wang SG, Fu CB, Chou JF (2008) An overview of the semi-arid climate and environment research observatory over the Loess Plateau. Adv Atmos Sci 25(6):906–921. https://doi.org/10.1007/s00376-008-0906-7

Huang J, Guan X, Ji F (2012) Enhanced cold-season warming in semi-arid regions. Atmos Chem Phys 12(2):4627–4653

Huang J, Ji M, Xie Y (2015) Global semi-arid climate change over last 60 years. Clim Dyn 46(3):1131–1150. https://doi.org/10.1007/s00382-015-2636-8

Li B, Zhang JD (2003) Analysis of relationships between vegetation and climate variables in Loess Plateau. Acta Ecol Sin 23(1):82–89. https://doi.org/10.3321/j.issn:1000-0933.2003.01.011

Li GP, Zhao BJ, Lu JH (2002) Characteristics of bulk transfer coefficients over the Tibetan Plateau. Acta Meteorol Sin 60(1):60–67

Li HY, Zhang Q, Shi JS, Zhao JH, Wang S (2012a) A study of the parameterization of land-surface processes over the natural vegetation surface of Loess Plateau. Acta Meteorol Sin 70(5):1137–1148

Li ZC, Wei ZG, Wang C, Zheng ZY, Wei H, Liu H (2012b) Simulation and improvement of common land model on the bare soil of Loess Plateau underlying surface. Sci China (Earth Sci) 66(4):1091–1097

Li DL, Shao PC, Wang H (2013) The positon variations of the north boundary of east Asian subtropical summer monsoon in 1951–2009. J Desert Res 33(5):1511–1519

Lin S, Wang YR (2007) Spatial-temporal evolution of precipitation in China Loess Plateau. J Desert Res 27(3):502–508

Liu CZ (2004) The issues in the impact study of climate change on the terrestrial hydrological cycle. Adv Earth Sci 19(1):115–119

Liu ZH, Tu G, Dong WJ (2008) Variability of surface albedo among different underlying surfaces in semi-arid region. Sci Bull 53:1220–1227

Liu ZG, Shao QQ, Tao J, Chi WF (2015) Intra-annual variability of satellite observed surface albedo associated with typical land cover types in China. J Geogr Sci 25(1):35–44

Ma YM, Kang S, Zhu L, Xu B, Tian L, Yao T (2008) Tibetan observation and research platform-atmosphere–land interaction over a heterogeneous landscape. Bull Am Meteorol Soc 89(10):1487–1492

Monin AS, Obukhov AM (1959) Basic laws of turbulent mixing in the surface layer of the atmosphere. Trudy Geofiz Inst AN SSSR 64:1963–1987

Nachtergaele F, Velthuizen HV, Verelst L (2008) Harmonized world soil database. Food and Agriculture Organization of the United Nations, Rome

Nicholson SE (2015) Evolution and state of our understanding of the role played in the climate system by land surface processes in semi-arid regions. Glob Planet Change 133:201–222. https://doi.org/10.1016/j.gloplacha.2015.08.010

Oke TR (1978) Boundary Layer climate. London Methuen & COLTD, New York, pp 31–66

Ou TH, Qian WH (2006) Vegetation variations along the monsoon boundary zone in East Asia. Chin J Geophys 49(3):698–705

Rechid D, Raddatz JT, Jacob D (2009) Parameterization of snow-free land surface albedo as a function of vegetation phenology based on MODIS data and applied in climate modelling. Theor Appl Climatol 95(3):245–255

Stull RB (1988) An introduction to boundary layer meteorology. Kluwer Academic Publishers, Dordrecht, p 666

Stull RB (2005) Meteorology for scientists and engineers. Brooks/Cole Thomson Learning, Pacific Grove, p 580

Sun BQ, Zhang Q, Dong AX, Chen SY (2005) Evolution feature on the moisture of soil for Loess Plateau in Gansu. Adv Earth Sci 20(9):1041–1046

Tang XG, Sun W, Qian WH (2007) North edge study of the Asian summer monsoon. China Meteorological Press, Beijing, p 96

Wang CH, Huang BX, Yang XG (2007) A Study on surface flux and the bulk transfer coefficients over middle Gansu region of Loess Plateau under the wheat and bare fields. Plateau Meteorol 26(1):30–38

Wang G, Huang J, Guo W (2010) Observation analysis of land-atmosphere interactions over the Loess Plateau of northwest China. J Geophys Res 115:D00K17

Wang YP, Kowalczyk E, Leuning R, Abramowitz G, Raupach MR, Pak B, Gorsel EV, Luhar A (2011) Diagnosing errors in a land surface model (CABLE) in the time and frequency domains. J Geophys Res 116(G1):G01034. https://doi.org/10.1029/2010JG001385

Wang WY, Zhang Q, Yang FL (2013) Study of the minimum available precipitation and the precipitation conversion rate in the semi-arid Yuzhong region. Acta Meteorol Sin 71(5):952–961

Zeng QC, Wang HJ, Lin ZH, Li CY, Huang RH, Wu GX, Zhou TJ (2003) A study of the climate dynamics and climate prediction theory. Chin J Atmos Sci 27(4):468–483

Zeng J, Zhang Q, Wang S (2011) Regional differences in the characteristics of clear-sky land surface processes in distinct climatic zones over northern China. Chin J Atmos Sci 35(3):483–492

Zhang Q, Huang RH (2004) Water vapor exchange between soil and atmosphere over a gobi surface near an oasis in summer. J Appl Meteorol 43(12):1917–1928

Zhang Q, Wang S (2008) On land surface processes and its experimental study in Chinese Loess Plateau. Adv Earth Sci 23(2):167–173

Zhang Q, Hu YQ, Cao XY, Liu WM (2000) On some problems of arid climate system of northwest China. J Desert Res 20(4):357–362

Zhang Q, Wei GA, Huang RH, Cao XY (2002a) Bulk transfer coefficients of the atmospheric momentum and sensible heat over desert and Gobi in arid climate region of Northwest China. Sci China (Earth Sci) 45(5):468–480

Zhang Q, Wei GA, Cao XY, Huang RH (2002b) Observation and study of land surface parameters over Gobi in typical arid region. Adv Atmos Sci 19(1):121–135

Zhang Q, Deng ZY, Zhao YD, Qiao J (2008) The impacts of global climatic change on the agriculture in northwest China. Acta Ecol Sin 28(3):1210–1218

Zhang Q, Hu XJ, Wang S, Liu HY, Zhang J, Wang RY (2009a) Some technological and scientific issues about the experimental study of land surface processes in Chinese Loess Plateau (LOPEX). Adv Earth Sci 24(4):363–371

Zhang Q, Wang S, Zhang J, Wang RY, Liu HY, Li YY (2009b) The progresses on land surface processes and atmospheric boundary layer in arid regions. Adv Earth Sci 24(11):1185–1194

Zhang Q, Zeng J, Yao T (2012a) Interaction of aerodynamic roughness length and wind flow conditions and its parameterization over vegetation surface. Sci China (Earth Sci) 57(13):1559–1567

Zhang Q, Li HY, Zhao JH (2012b) Modification of the land surface energy balance relationship by introducing vertical sensible heat advection and soil heat storage over the Loess Plateau. Sci China (Earth Sci) 55(4):580–589. https://doi.org/10.1007/s11430-011-4220-3

Zhang Q, Zeng J, Zhang LY (2012c) Characteristics of land surface thermal-hydrologic processes for different regions over North China during prevailing summer monsoon period. Sci China (Earth Sci) 55(11):1872–1880. https://doi.org/10.1007/s11430-012-4373-8

Zhang Q, Huang J, Zhang L, Zhang LY (2013a) Warming and drying climate over Loess plateau area in China and its effect on land surface energy exchange. Acta Phys Sin 62(13):139202

Zhang Q, Li HY, Zhang LY, Yue P, Shi JS (2013b) Responses of the land-surface process and its parameters over the natural vegetation underlying surface of the middle of Gansu in loess plateau to precipitation fluctuation. Acta Phys Sin 62(1):019201

Zhao SC (2002) Front scientific problems of global change and China's water cycle. Adv Earth Sci 17:628–730

Zheng Y, Kumar A, Niyogi D (2015) Impacts of land–atmosphere coupling on regional rainfall and convection. Clim Dyn 44(9):2383–2409

Zhou YL, Sun XM, Zhu ZL, Zhang RH, Tian J, Lu YF, Guan DX, Yuan GF (2006) Surface roughness length dynamic over several different surfaces and its effects on modeling fluxes. Sci China (Earth Sci) 49(S2):262–272